

Beyond maps: Patterns of formation processes at the Middle Pleistocene open-air site of Marathousa 1, Megalopolis Basin, Greece

D. Giusti^{a,*}, V. Tourloukis^a, G. E. Konidaris^a, N. Thompson^a, P. Karkanas^c,
E. Panagopoulou^d, K. Harvati^a

^a*Paläoanthropologie, Senckenberg Centre for Human Evolution and Palaeoenvironment, Eberhard Karls Universität Tübingen, Rümelinstr. 23, 72070 Tübingen, Germany*

^b*Friedrich-Alexander University of Erlangen-Nürnberg, Institute of Prehistory and Early History, Kochstr. 4/18, 90154 Erlangen, Germany*

^c*Malcolm H. Wiener Laboratory for Archaeological Science, American School of Classical Studies at Athens, Greece*

^d*Ephoreia of Palaeoanthropology-Speleology of Greece, Athens, Greece*

Abstract

Recent excavations at the Middle Pleistocene open-air site of Marathousa 1 have unearthed in one of the two investigated areas (Area A) a partial skeleton of a single individual of *Elephas (Palaeoloxodon) antiquus* and other faunal remains in spatial and stratigraphic association with lithic artefacts. In Area B, a much higher number of lithic artefacts was collected, spatially and stratigraphically associated with other faunal remains. The two areas are stratigraphically correlated, the main fossiliferous layers representing an *en masse* depositional process in a lake margin context. Evidence of butchering (cut-marks) has been identified on two bones of the elephant skeleton, as well on other mammal bones from Area B. However, due to the secondary deposition of the main find-bearing units, it is of primary importance to evaluate the degree and reliability of the spatial association of the lithic artefacts with the faunal remains. Indeed, spatial association does not necessarily imply causation, since natural syn- and post-depositional processes may equally produce spatial association. Assessing the degree and extent of post-depositional reworking processes is crucial to fully comprehend the archaeological record, and therefore to reliably interpret past human behaviours. The present study uses a comprehensive set of spatial statistics in order to disentangle the depositional processes behind the distribution of the archaeological and palaeontological record at Marathousa 1. Preliminary results of our analyses suggest minor reworking and substantial spatial association of the lithic and faunal assemblages, supporting the current interpretation of Marathousa 1 as a butchering site.

Keywords: Spatial analysis, Site formation processes, Vertical distribution, Fabric analysis, Point pattern analysis, Middle Pleistocene

*Corresponding author

Email address: domenico.giusti@uni-tuebingen.de (D. Giusti)

1. Introduction

2 Archaeological site formation processes, intensively studied since the early 1970s
3 (Isaac, 1967; Schiffer, 1972, 1983, 1987; Shackley, 1978; Wood and Johnson, 1978; ?;
4 Schick, 1984, 1986, 1987; Petraglia and Nash, 1987; Petraglia and Potts, 1994, among
5 others), “still insufficiently taken in consideration” (Texier, 2000, p.379) at the be-
6 ginning of the 21st century, are nowadays fully acknowledged in the archaeological
7 practice (Villa, 2004; Bailey, 2007; Brantingham et al., 2007; Malinsky-Buller et al.,
8 2011; Vaquero et al., 2012; Bargalló et al., 2016, among others). Drawing inferences
9 about past human behaviours from scatters of archaeological remains must account for
10 syn- and post-depositional contextual processes.

11 Several methods are currently applied in order to qualify and quantify the type and
12 degree of reworking of archaeological assemblages. Within the framework of a geoar-
13 chaeological and taphonomic approach, spatial statistics offer meaningful contributions
14 in unravelling site formation and modification processes from spatial patterns. How-
15 ever, while the spatio-temporal dimension is an ineluctable inherent property of any
16 biotic or abiotic process, spatial statistics are still insufficiently applied.

17 Distribution maps are cornerstones of the archaeological documentation process
18 and are primary analytic tools. However, their visual interpretation is prone to subjec-
19 tivity and is not reproducible (Bevan et al., 2013). Since the early 1970's (see Hodder
20 and Orton (1976); Orton (1982) and references therein), the traditional, intuitive, ‘eye-
21 balling’ method of spotting spatial patterns has been abandoned in favour of more ob-
22 jective approaches, extensively borrowed from other fields. Nevertheless, quantitative
23 methods, while still percolating in the archaeological sciences from neighbouring dis-
24 ciplines, are not extensively used. Moreover, only a relatively small number of studies
25 have explicitly applied spatial point pattern analysis or geostatistics to the study of site
26 formation and modification processes (Lenoble et al. (2008); Domínguez-Rodrigo et al.
27 (2014b,a, 2017); Carrer (2015); Giusti and Arzarello (2016); Organista et al. (2017) -
28 but see Hivernel and Hodder (1984) for an earlier work on the subject).

29 The goal of a taphonomic approach to spatial analysis is to move beyond distri-
30 bution maps by applying a comprehensive set of multiscale and multivariate spatial
31 statistics in order to reliably construct inferences from spatial patterns. An exhaustive
32 spatial analytic approach to archaeological inference, combined with a taphonomic
33 perspective, is essential for evaluating the depositional processes and integrity of the
34 archaeological assemblage, and consequently for a reliable interpretation of past hu-
35 man behaviours.

36 The present study uses a comprehensive set of spatial statistics in order to disentan-
37 gle the depositional processes behind the spatial distribution of the archaeological and
38 palaeontological record recovered during excavation at the Middle Pleistocene open-air
39 site of Marathousa 1, Megalopolis, Greece (Panagopoulou et al., 2015; Harvati et al.,
40 2016).

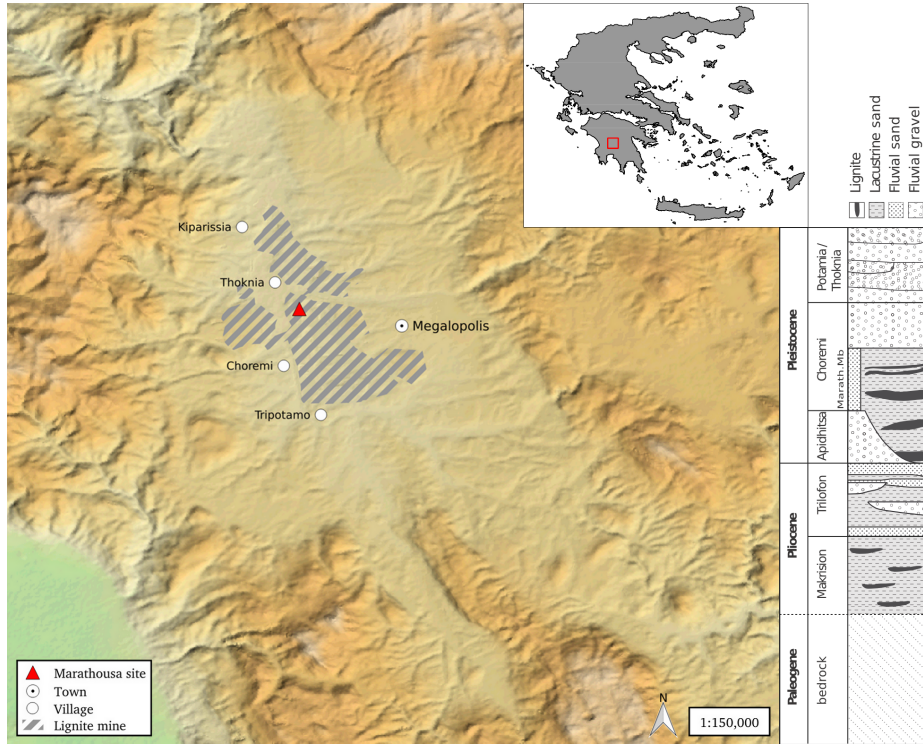


Figure 1: Geographical location of the Marathousa 1 site in the Megalopolis basin and stratigraphic column, modified after [van Vugt et al. \(2000\)](#).

41 1.1. Marathousa 1

42 The site (Fig. 1), discovered in 2013 at the edge of an active lignite quarry (Thompson et al., this issue), is located between two lignite seams in the Pleistocene deposits
 43 of the Megalopolis basin, Marathousa Member of the Choromai Formation ([van Vugt](#)
 44 et al., 2000). The regular alternation of lacustrine clay, silt and sand beds with lignite
 45 seams has been interpreted having cyclic glacial (or stadial) and interglacial (or inter-
 46 stadial) origin (Nickel et al., 1996). The half-graben configuration of the basin, with
 47 major subsidence along the NW-SE trending normal faults along the eastern margin,
 48 resulted in the gentle dip of the lake bottom at the opposite, western, margin of the
 49 lake, enabling the formation of swamps and the accumulation of organic material for
 50 prolonged periods of time ([van Vugt et al., 2000](#)).
 51

52 Two excavation areas have been investigated since 2013 (Fig. ??): Area A, where
 53 several skeletal elements of a single individual of *Elephas (Palaeoloxodon) antiquus*
 54 have been unearthed, together with a number of lithic artefacts; and Area B, located
 55 60 m to the South along the exposed section, where the lithic assemblage is richer and
 56 occurs in association with a faunal assemblage composed of isolated elephant bones,
 57 cervids and carnivores among others (Konidaris et al., this issue; Touloukis et al.,
 58 this issue). Evidence of butchering (cut-marks) have been identified on two of the

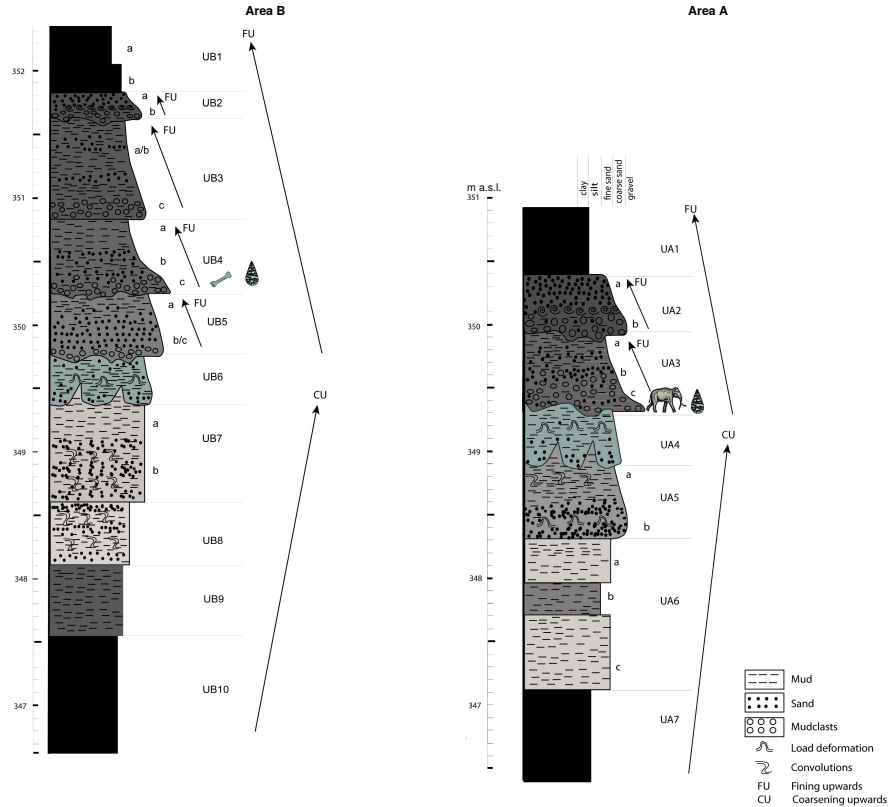


Figure 2: Stratigraphic setting of the Marathousa 1 site, modified after Karkanas et al. (this issue).

59 elephant bones from Area A, as well on elephant and other mammal bones from Area
60 B (Konidaris et al., this issue).

61 The sedimentary sequence of the site (Fig. 2) includes lacustrine and fluvio-lacustrine
62 clastic deposits between lignite seam II (UA7-UB10) and the lower part of seam III
63 (UA1-UB1) (Karkanas et al., this issue; Tourloukis et al., this issue). A major hiatus
64 (UA3/4, UB5/6), attributed to exposure and erosion of a lake shore mudflat, divides
65 the sequence in two parts. The lower part is characterized by relatively high rate sub-
66 aqueous sedimentation of bedded sands and silts, containing low organic and carbonate
67 content. The upper one is characterized by a series of erosional bounded depositional
68 units, attributed to subaerial organic- and carbonate-rich mudflows and hyperconcen-
69 trated flows (Karkanas et al., this issue).

70 The erosional contacts UA3c/4 and UB4c/5a separate the two main find-bearing
71 units in both areas. In Area A, the elephant remains lie at the contact of UA3c/4 and
72 are covered by UA3c (Fig. 3a); while in Area B, most of the remains were collected
73 from unit UB4c (Fig. 3b). Units UA3c and UB4c (organic- and intraclast-rich silty

sands) resemble dilute mudflows, showing a chaotic structure of rip-up clasts from the underlying unit, small-to-large wood fragments and rare rock clasts. In Area B, a relatively low number of remains was also found in massive organic-rich silty sands (UB5a), which locally overlay channalized sands (UB5b/c), probably not preserved in Area A (Karkanas et al., this issue).

The flow event described above (units UA3c and UB4c), and specifically the erosional contacts between the fossiliferous horizons in the two areas (UA3c/4 and UB4c/5a), provide the essential background for the analysis and interpretation of the spatial distributions at Marathousa 1.

The secondary depositional nature of the main find horizons raises the question of how reliable is the spatial association between the lithic artefacts and the partial skeleton of a single *Elephas (Palaeoloxodon) antiquus* individual and other faunal remains. Since spatial association does not necessarily imply causation, and consequently synchrony, the answer has important consequences for the interpretation of the site in the broader context of the Middle Pleistocene human-proboscidean interactions. We aim to tackle this question and disentangle the formation processes acting at Marathousa 1 on the basis of spatial patterns through a three-prong spatial analytic approach:

1. by analysing, in a frame of references, the orientation patterns of remains from relevant stratigraphic units;
2. by quantifying and comparing their relative vertical distributions;
3. by identifying spatial trends in either the assemblage intensities and the associations between classes of remains.

For both areas, the working hypothesis is that the flow event, represented by units UA3c and UB4c, eroded and scoured the exposed surface (where the elephant was lying), thereby entraining clastic material (including probably artefacts) and re-depositing this material at a close distance. Two contrasting models are tested: the autochthonous model ([Domínguez-Rodrigo et al., 2012](#), sensu) states that the post-depositional UA3c-UB4c flow reworked *on site* the assemblage and altered the original, pristine *in situ* deposition. This model implies the loss of any primary spatial relations between remains and minor transport from the primary depositional *loci*. On the other hand, the allochthonous model ([Domínguez-Rodrigo et al., 2012](#), sensu) implies significant transport from the original *loci* and re-elaboration. According to this model, the spurious spatial association between the lithic artefacts and faunal remains does not support any behavioural interpretation.

2. Material and methods

Since 2013, systematic investigation of the Marathousa 1 site has been carried out by a joint team from the Ephoreia of Palaeoanthropology-Speleology (Greek Ministry of Culture) and the University of Tübingen. A grid system of 1 square meter units was set up, oriented -14 degrees off the magnetic North, and including the two areas of investigation. The excavation of the deposit proceeded in 50x50 cm sub-squares in Area B and 1x1 m squares in Area A, and spits of 5 to 10 cm thickness, respectively. Systematic water-screening of sediments was carried out on-site using 1 mm



Figure 3: Photograph (2017) of the left femur of the *Elephas (Palaeoloxodon) antiquus*, lying at the contact of UA3c/4 and covered by UA3c (a). West profile (2014) of the excavation Area B, exposing the UB4c/5a and UB5c/6 erosional contacts (b).

116 sieves in order to guarantee recovery of the small-size fraction (e.g., micro-artefacts,
117 small mammal remains, fish, molluscs and small fragments of organic and inorganic
118 material). The three-dimensional coordinates of finds (i.e., all the lithic artefacts, teeth
119 and diagnostic bones; bones and organic material with a-axis \geq 20 mm), collected
120 spits of sediment, samples and geological features (e.g., erosional contacts and mud
121 cracks) were recorded with a Total Station. Dense clouds of surface points of the Ele-
122 phant skeletal elements were acquired using both a Total Station and a close-range
123 photogrammetric technique.

124 The dimensions (length, width and thickness) of registered finds were measured
125 on-site with millimetre rules. Orientation (dip and strike) of elongated particles (i.e.,
126 faunal remains, large wood fragments and lithic artefacts) was recorded since 2013
127 with a 30 degree accuracy, using a clock-like system (the strike was measured, rela-
128 tively to the grid North, in twelve clockwise intervals). In 2015, the use of a compass
129 and inclinometer with an accuracy of 1 degree was introduced in Area B to gradually
130 replace the former method.

131 The widespread use of a compass and inclinometer to record orientation data (Voorhies,
132 1966; Bertran and Texier, 1995; Bertran et al., 1997; Lenoble and Bertran, 2004; ?;
133 Eren et al., 2010; Benito-Calvo et al., 2011; Domínguez-Rodrigo et al., 2012; Domínguez-
134 Rodrigo and García-Pérez, 2013; Domínguez-Rodrigo et al., 2014c; Cobo-Sánchez
135 et al., 2014; Organista et al., 2017, among others) was favoured over the alternative
136 use of a total station (??McPherron, 2005; ?; Bernatchez, 2010, among others), mostly
137 due to the time-restricted conditions of the rescue excavation conducted at Marathousa
138 1.

139 Measurements of the strike (azimuth) and dip of elongated finds were taken along
140 the symmetrical longitudinal a-axis (SLA) of bones (Domínguez-Rodrigo and García-
141 Pérez, 2013), lithic artefacts (Bertran and Texier, 1995) and organic material, using the
142 lowest endpoint of the axis as an indicator of the vector direction.

143 Other major axes have been alternatively used with the recent application of GIS
144 techniques to retrieve orientation data from secondary source (i.e., excavation pho-
145 tographs, drawings or maps) (Boschian and Saccà, 2010; Benito-Calvo and de la Torre,
146 2011; de la Torre and Benito-Calvo, 2013; Walter and Trauth, 2013; García-Moreno
147 et al., 2016; Sánchez-Romero et al., 2016). However, the experimental works of Domínguez-
148 Rodrigo and García-Pérez (2013) and Domínguez-Rodrigo et al. (2014c) showed that
149 the SLA, defined as the major axis which symmetrically divide the bone, is more ac-
150 curate in determining the preferential orientation of anisotropic assemblages. This a-
151 axis is commonly used in taphonomic studies (??Domínguez-Rodrigo et al., 2012,
152 2014a; ?, among others) and, not explicitly defined but commonly referred to as the
153 clast/artefact long or major axis, in studies which employ a sedimentological approach
154 to archaeological fabric (Bertran and Texier, 1995; Bertran et al., 1997; Lenoble and
155 Bertran, 2004; Benito-Calvo et al., 2009, among others).

156 The present study focuses on the excavated stratigraphic units in which most of the
157 archaeological and palaeontological remains were recovered in both excavation areas,
158 namely in UA3c and UA4 in Area A, and UB4c and UB5a in Area B. From the total,
159 subset samples of material were used for each specific spatial analysis. For the fabric
160 analysis we included material collected until 2016. For the vertical distribution and
161 point pattern analyses, the region of investigation was limited to the squares excavated

162 from 2013 until 2015, 25 and 29 square meters respectively in each area.

163 The analyses were performed in R statistical software ([R Core Team, 2016](#)). In
164 order to make this research reproducible ([Marwick, 2017](#); [Marwick et al., 2017](#)), a
165 repository containing a compendium of data, source code and text is open licensed and
166 available at the DOI: [10.5281/zenodo.822273](https://doi.org/10.5281/zenodo.822273)

167 *2.1. Fabric analysis*

168 The study of the clast fabric (i.e., the orientation pattern of elongated sedimentary
169 particles, including bones and artefacts), first addressed by [Voorhies \(1966\)](#); [Isaac](#)
170 ([1967](#)); [Bar-Yosef and Tchernov \(1972\)](#); [Schick \(1986\)](#), more recently led to a note-
171 worthy development of methods and propagation of applications in Palaeolithic site
172 formation studies ([Bertran and Texier, 1995](#); [Bertran et al., 1997](#); [Lenoble and Bertran,](#)
173 [2004](#); [Lenoble et al., 2008](#); [McPherron, 2005](#); [Benito-Calvo et al., 2009, 2011](#); [Benito-](#)
174 [Calvo and de la Torre, 2011](#); [Bernatchez, 2010](#); [Boschian and Saccà, 2010](#); [Domínguez-](#)
175 [Rodrigo et al., 2012](#); [Domínguez-Rodrigo and García-Pérez, 2013](#); [Domínguez-Rodrigo](#)
176 [et al., 2014c](#); [de la Torre and Benito-Calvo, 2013](#); [Walter and Trauth, 2013](#); [García-](#)
177 [Moreno et al., 2016](#); [Sánchez-Romero et al., 2016](#), among others).

178 Fabric analysis can provide valuable insight into site formation and taphonomic
179 processes, allowing discrimination between orientation patterns (isotropic, linear or
180 planar) associated with different sedimentary processes. Whereas water-flow deposits
181 are, in general, characterized by relatively good sorting and preferred orientation of
182 clasts parallel, or normal to the flow direction (linear fabric) ([Petalglia and Potts, 1994](#));
183 debris-flow deposits generally exhibit massive, poorly bedded mixtures of unsorted
184 sediments and random orientation of clasts (isotropic fabric), except at the flow margins
185 ([Pierson, 2005](#)). On the other hand, undisturbed archaeological sites, as well as exper-
186 imental sites, have been observed to have planar fabric ([Bertran et al., 1997](#); [Lenoble and](#)
187 [Bertran, 2004](#)). Nevertheless, grey zones exist between depositional processes, so that
188 an unequivocal discrimination based only on fabric observations is often not possible,
189 and other taphonomic criteria must also be considered ([Lenoble and Bertran, 2004](#)). As
190 an example, while overland flows (runoff) have been observed to show planar fabrics
191 ([Lenoble and Bertran, 2004](#)), anisotropy without significant transport can be caused in
192 a lacustrine floodplain by low-energy processes such as lake transgression and regres-
193 sion, as well as water-sheet flows formed during rainy seasons ([Cobo-Sánchez et al.,](#)
194 [2014](#)).

195 At the margin of a lacustrine environment, relatively close to the surrounding re-
196 lief, a combination of high- and low-energy processes can be expected. According to
197 the sedimentological and micromorphological study of the Marathousa 1 site, mud-
198 flows and hyperconcentrated flows are associated with the main find-bearing horizons
199 (Karkanas et al., this issue). Hyperconcentrated flows are intermediate states, defined
200 by sediment concentration, in the continuum between subaerial water flows and de-
201 bris flows. ? report that, when a turbulent fluidal flow expands over a surface - as in
202 the case of Marathousa 1 - a two-phase flow may develop, with a more concentrated,
203 coarser grained bottom flow-layer (traction carpet) moving slower than the upper tur-
204 bulent flow-layer carrying washload and suspended load. Resultant deposit may exhibit
205 diagnostic inverse grading (?), or a continuously aggrading bed (?). Parallel or normal

Table 1: List of sampled observations for the fabric analysis.

Sample	<i>n</i>	Type		
		Fauna	Wood	Lithic
UA3c	49	23	25	1
UA4	38	8	30	-
<i>E. (P.) antiquus</i>	63			
UB4c	38	30	1	7

206 orientation of the clast to the flow direction can be observed (?). Moreover, a simulation
 207 model showed that linear fabric can develop in mudflows as well. However, after
 208 deposition, settling of the clasts may affect the fabric to some extent, depending on the
 209 viscosity of the mudflow (?).

210 As part of our three-prong spatial analytic approach, we conducted comparative
 211 fabric analysis with the aim to investigate the dynamics of the depositional processes
 212 at Marathousa 1.

213 Since fabric strength has been found to be positively correlated with the shape
 214 and size of the clast, for the fabric analysis we subset samples of remains with length
 215 ≥ 2 cm and elongation index (the ratio length/width) $I_e \geq 1.6$ ([Lenoble and Bertran, 2004](#)). The samples are listed in Table 1 and include mostly wood fragments and faunal
 216 remains from the four stratigraphic units under investigation. No distinction of skeletal
 217 elements was made, both due to the high fragmentation rate of faunal remains in Area
 218 B, and because recent experiments showed a similar orientation pattern for different
 219 bone shapes ([Domínguez-Rodrigo et al., 2012](#); [Domínguez-Rodrigo and García-Pérez, 2013](#)).
 220

221 The sample of bones belonging to the individual of *Elephas (P.) antiquus* from
 222 Area A was analysed separately and included the humerus, ulna, femur and tibia; the
 223 atlas, axis and 16 complete vertebrae or vertebral fragments; 29 complete ribs or rib
 224 fragments; 2 calcanea; 4 metatarsals/metacarpals; the pyramidal; the trapezoid and the
 225 pelvis. The sample from UB5a was too small (only 7 observations) and was therefore
 226 excluded. In order to asses the reliability of the orientation data recorded using the
 227 clock method, we analysed two sub-samples from unit UB4c, selected from a set of
 228 finds recorded using both methods. All the sampled observations are representative of
 229 the whole study area.
 230

231 Rose diagrams and uniformity tests, such as Rayleigh, Kuiper, Watson and Rao
 232 tests ([Jammalamadaka et al., 2001](#)), were used to visualise and evaluate circular isotropy
 233 in the sample distribution. The Rayleigh test is used to assess the significance of the
 234 sample mean resultant length (\bar{R}), assuming that the distribution is unimodal and not
 235 bi- or plurimodal. The \bar{R} ranges from 0 to 1: values close to 1 indicate that the data are
 236 closely clustered around the mean direction; when the data are evenly spread \bar{R} has a
 237 value close to 0. A p -value lower than 0.05 rejects the hypothesis of randomness with
 238 a 95% confidence interval. Kuiper, Watson and Rao are omnibus tests used to detect
 239 multimodal departures from circular uniformity. The Watson's goodness of fit test was
 240 conducted for the von Mises distribution (circular normal distribution). The test results
 241 are evaluated against critical values: a result higher than the critical value rejects with
 242 confidence the null hypothesis.

243 Randomness testing of three-dimensional data was conducted with the Woodcock
244 S_1/S_3 test (Woodcock and Naylor, 1983). Considering both the dip (plunge) and strike
245 (bearing) of the oriented items, this method, based on three ordered eigenvalues (S_1 ,
246 S_2 , S_3), is able to discriminate the shape and strength of the distributions. The shape
247 parameter $K = \frac{\ln(S_1/S_2)}{\ln(S_2/S_3)}$ ranges from zero (uni-axial girdles) to infinite (uni-axial clus-
248 ters). The parameter $C = \ln(S_1/S_3)$ expresses the strength of the preferential orienta-
249 tion, and its significance is evaluated against critical values from simulated random
250 samples of different sizes. A perfect random uniform distribution would have $C = 0$
251 and $K = 1$.

252 The Benn (Benn, 1994) diagram adds to the Woodcock test an isotropy ($IS =$
253 S_3/S_1) and an elongation ($ES = 1 - (S_2/S_1)$) index. Like the former method, it is
254 able to differentiate between linear (cluster), planar (girdle) or isotropic distributions.
255 There are no published raw data from actualistic studies on hyperconcentrated flows or
256 other depositional processes affecting the orientation of bones and artefacts deposited
257 on lacustrine floodplains (but see Morton (2004) and Cobo-Sánchez et al. (2014) as
258 pioneer studies on this subject). However, we included in the Benn diagram references
259 to published results from observation of fabrics in modern subaereal slope deposits,
260 i.e., debris flow and runoff (Bertran et al., 1997; Lenoble and Bertran, 2004).

261 2.2. Vertical distribution

262 The vertical distribution of materials has been long investigated with the aim of
263 identifying cultural levels, by visually interpreting cross-sectional plots. However, re-
264 cent advances in GIS techniques allow to quantitatively inspect at higher resolution
265 the three-dimensional distributions of archaeological remains (?Anderson and Burke,
266 2008, among others).

267 In analysing the vertical dispersion of material at Marathousa 1, we provisionally
268 assume that a general concentration of unsorted lithic artefacts and faunal remains in
269 the proximity of the erosional surfaces would support an autochthonous origin of the
270 assemblages; whereas a homogeneous vertical distribution of remains from the UA3c
271 and UB4c units would suggest an allochthonous origin, significant transport and sub-
272 sequent redeposition of the material. Indeed, massive process such as mudflows or hy-
273 perconcentrated flows, have high erosional power and rather chaotic structure, which
274 would result in inverse (?) or normal grading (?).

275 In order to estimate the degree of vertical dispersion while controlling for the size
276 of the archaeological material, dimensional classes were set up following typological
277 criteria. Lithic artefacts were classified as debris/chips when smaller than a cutoff
278 length of 15 mm (see Tourloukis et al., this issue). Other classes include flakes, tools
279 and cores; the latter being the bigger and heavier debitage product. Table 2 summarises
280 the sample size for each class. Lithic debris/chips constitutes the larger part of the
281 assemblages from UB4c (60%) and UB5a (49%); whereas in Area A it represents only
282 a moderate percentage in the upper UA3c unit (16%). The very rare presence of lithic
283 artefacts in the underlying unit UA4 is nevertheless significant. In this unit, the faunal
284 remains are also found in much lower numbers, their number reduced to one fourth
285 of those found in UA3c. For the point pattern analysis (see below), we used the same
286 subset of materials for both excavation areas.

Table 2: List of sampled observations for the vertical distribution and point pattern analyses.

Sample	<i>n</i>	Lithic class					Faunal class			
		Debris/chip	Flake	Bone flake	Tool	Core	Indet.	Bone	Tooth	Microfauna
UA3c	279	46	2	-	1	-	1	171	14	44
UA4	61	3	1	-	-	-	-	45	4	8
UB4c	1243	753	154	1	34	6	2	246	28	19
UB5a	101	50	12	-	3	-	-	30	3	3

287 For Area B, the material recovered from the water-screening was randomly provenanced according to the 5 cm depth of the excavated spit and the coordinates of the
 288 50x50 cm quadrant of the excavation square. Following the same excavation protocol,
 289 the same procedure was applied for the water-screened material of Area A, which was
 290 randomly provenanced according to 3D-coordinates of the 1x1 m excavation square
 291 and 10 cm spit.
 292

293 Ordinary Kriging interpolation of the recorded points of contact between the UA3c/UA4
 294 and UB4c/UB5a stratigraphic units were used to reconstruct the UA3c/4 and UB4c/5a
 295 erosional surface (Fig. 4a,b). In geostatistics, Kriging is a method of interpolation
 296 which, from a modelled function of spatial autocorrelation between known points (e.g.,
 297 recorded elevations), calculates values of unknown points (e.g., predicted elevations).
 298 Thus, in order to address our specific objective, i.e., to quantify and analyse the verti-
 299 cal distribution of the archaeological and palaeontological material, we measured the
 300 minimum orthogonal distance of each specimen to the interpolated erosional surface
 301 (Fig. 4c). For the units above and below this surface (i.e., UB4c and UB5a), the rela-
 302 tive distribution of lithic classes and faunal remains was informally tested by means of
 303 kernel density estimations.

304 In Area A, the UA3c/4 erosional surface is mixed, rather than sharp: remains of
 305 the eroded unit UA4 are mixed with pockets of the UA3c organic-rich silty sands and
 306 intraclast-rich mudflows (Karkanas et al., this issue). However, from sparse known
 307 points, the UA3c/4 surface was interpolated and the vertical dispersion of remains es-
 308 timated. The elephant remains were excluded from this analysis, since they clearly lie
 309 horizontally at the UA3c/4 contact (Fig. 3a and SI).

310 Finally, a Student's two sample t-test allowed us to compare the empirical distribu-
 311 tions of different groups of remains for each stratigraphic unit.

312 2.3. Point pattern analysis

313 A spatial point pattern is defined as the outcome of a random spatial point process
 314 (repetitions of it would always create a different pattern). The observed patterns of the
 315 archaeological and palaeontological remains were treated as manifestations of spatial
 316 point processes, i.e., site formation processes. Point pattern analysis investigates the
 317 spatial arrangement of points with the aim of identifying spatial trends. In order to
 318 integrate the previous studies of the fabric and vertical distributions, we directed our
 319 point pattern analysis equally to the intensity of the patterns (the rate of occurrence of
 320 the recorded finds) and to the spatial interaction between different types of finds.

321 As the average number of random points per unit area, intensity informs about ho-
 322 mogeneity or inhomogeneity in the distribution of events generated by a point process,

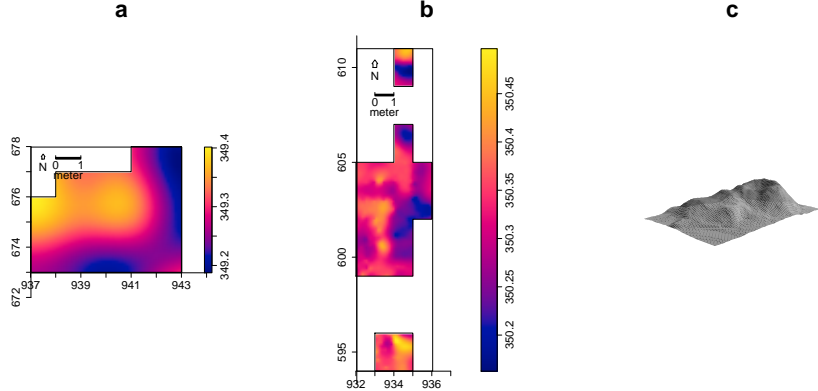


Figure 4: Ordinary Kriging interpolation of the UA3c/4 (a) and UB4c/5a (b) erosional surface; the color scale denotes elevation a.s.l. Illustration of the method used to quantify the vertical dispersion of remains with respect to the UB4c/5a surface (c).

i.e., whether the rate of occurrence is uniform or spatially varying across the study area. Intensity, usually non-parametrically evaluated by means of kernel density estimation (Diggle, 1985), was assessed for the distribution of material from the UB4c, UB5a and UA3c units. Cross-validation bandwidth, which assumes a Cox process, and edge correction were applied using the methods described in Diggle (1985).

In the presence of a covariate, it is recommended to further investigate the dependence of intensity on that explanatory variable. In order to evaluate whether variation in the density of materials was correlated to the topography of the erosional surface, we computed a local likelihood smoothing estimate of the intensity of remains from UB4c as a function of the UB4c/5a surface elevation model (Baddeley et al., 2012). Formal tests enabled us to assess the evidence of that dependence and to quantify the strength of the covariate. The Kolmogorov-Smirnov test of CSR (Complete Spatial Randomness) and Berman's Z_2 statistics were used to test the strength of evidence for a covariate effect. The Receiver Operating Characteristic (ROC) plot, and the area under the ROC curve (AUC), closely related to Berman's Z_2 test, measure the magnitude of the covariate effect. AUC values close to 1 or 0 indicate strong discrimination, whereas intermediate values (0.5) suggest no discrimination power.

Whereas intensity is a first-order property of the point process, multiscale inter-point interaction is measured by second or higher-order moment quantities, such as the Ripley's K correlation function (Ripley, 1976, 1977) and the distance G -, F - and J -functions. Three different types of inter-point interaction are possible: random, regular or cluster. In a hypothesis-testing framework, pointwise envelopes are computed by a number (199) of random simulations of the null hypothesis (i.e., random/Poisson distribution). Thus, values of the empirical distribution (black solid line) are plotted against the benchmark value (red dotted line) and the envelopes (grey area) which specify the critical points for a Monte Carlo test (Ripley, 1981). Regular patterns are

349 assumed to be the result of inhibition processes, while cluster patterns are the result of
350 attraction processes.

351 In order to test the spatial interaction between remains associated with the erosional
352 event of UB4c and those associated with the underlying UB5a unit, we treated the data
353 as a multivariate point pattern, assuming that the point patterns in UB4c and UB5a are
354 expressions of two different stationary point processes, i.e., depositional events. We
355 performed a cross-type pair correlation function ($g_{ij}(r)$), derivative of the multitype
356 $K_{ij}(r)$ function, which is the expected number of points of type j lying at a distance
357 r of a typical point of type i . The function is a multiscale measurement of the spatial
358 dependence between types i (UB4c) and j (UB5a). Randomly shifting each of the
359 two patterns, independently of each other, estimated values of $\hat{g}_{ij}(r)$ are compared to
360 a benchmark value $g_{ij}(r) = 1$, which is consistent with independence or at least with
361 lack of correlation between the two point processes.

362 In order to reduce the edge effect bias in estimating the correlation between points,
363 we implemented Ripley's isotropic edge correction (Ohsen, 1983; Ripley, 1988).

364 In addition to the pair correlation function, the multitype nearest-neighbour $G_{ij}(r)$
365 function was used to estimate the cumulative distribution of the distance from a point of
366 type i (UB4c) to the nearest point of type j (UB5a). It measures the spatial association
367 between the two assemblages. For the cross-type G -function, the null hypothesis states
368 that the points of type j follow a Poisson (random) distribution in addition to being
369 independent of the points of type i . Thus, in a randomisation technique, when the solid
370 line of the observed distribution ($\hat{G}_{ij}(r)$) is above or below the shaded grey area, the
371 pattern is significantly consistent with clustering or segregation, respectively. Complete
372 spatial randomness and independence (CSRI) of the two point processes would support
373 an allochthonous origin hypothesis for the assemblage recovered from the UB4c unit.
374 On the other hand, positive or negative association can be interpreted as expression of
375 different autochthonous processes.

376 The particle size spatial distribution of the lithic assemblage from UB4c was investi-
377 gated by means of a transformation of the multitype K -function ($K_{i\bullet}(r) - K(r)$, see
378 Baddeley et al. (2015), p.608). In this case, we treated the data as the manifestation of a
379 single multitype point process. In a joint distribution analysis, the locations and types
380 of points are assumed to be generated at the same time. The null model of a random
381 labelling test states that the type of each point is determined at random, independently
382 of other points, with fixed probabilities. The estimated K -function for a subset of pos-
383 sible combinations was evaluated against the envelope of Monte Carlo permutations of
384 the class of remains. Likewise with the vertical distribution, a horizontal clustering of
385 small specimens, such as lithic debris/chips, together with larger dimensional classes
386 of remains would suggest the lack of sorting by natural depositional processes.

387 As for the three-dimensional distribution of the lithic artefacts in Area A, and their
388 spatial association with the partial skeleton of the *E. (P.) antiquus*, we applied three-
389 dimensional univariate and bivariate second-order functions. A rectangular box of 20
390 square meters and 80 cm vertical extent was selected for the analyses (green outline in
391 Fig. ??a). Assuming homogeneity, the univariate pair correlation function ($g_3(r)$) was
392 estimated for the pattern of all the artefacts (mostly debris/chips) from UA3c and UA4.
393 In the specific context of the site, complete spatial randomness (CSR) would suggest
394 that the pattern most probably is the result of a random distribution process, such as

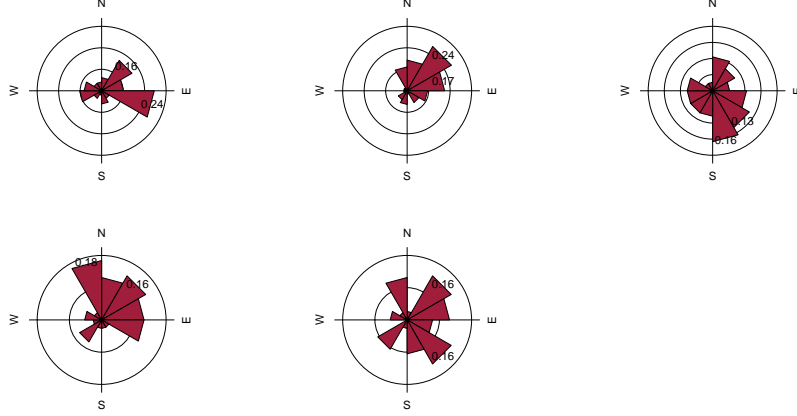


Figure 5: Rose diagrams showing the bearing patterns of samples from UA3c (a), UA4 (b), the elephant carcass (c) and UB4c (d: clock method, e: compass method).

395 a high energy mass movement. In contrast, other natural processes would produce
 396 clustering or segregation of the lithic artefacts. Spatial aggregation, if not generated by
 397 obstructions, would support an *in situ* primary origin of the assemblage.

398 In support to the pair correlation function, the cross-type nearest-neighbour function
 399 has been applied in order to compute, for each artefact recovered from the UA3c
 400 and UA4 units, the nearest point of the clouds of points associated with the elephant
 401 skeleton. A prevalence of short distances would indicate aggregation of the lithic arte-
 402 facts around the mass of the elephant; whereas a uniform or symmetric distribution
 403 would support random independent processes.

404 3. Results

405 3.1. Fabric analysis

406 The rose diagrams in Fig. 5 visualise the circular distributions of the examined
 407 specimens. Overall, the UA4 sample and the sample of elephant bones show predom-
 408 inant peaks in the NE quadrant; while the ones from units UA3c and UB4c suggest
 409 multimodal distributions. Specifically, the UA4 sample distribution (Fig. 5b) spreads
 410 largely in the NE quadrant. Similarly, the circular distribution of the elephant sam-
 411 ple (Fig. 5c), mainly lying in UA4, resembles the former distribution: it is skewed to
 412 the SW and concentrated in the NE quadrant. On the other hand, the UA3c sample
 413 (Fig. 5a) shows a plurimodal distribution with two peaks to the E and NE, and the two
 414 samples from Area B (Fig. 5d,e) suggest a different multimodal scenario.

415 Table 3 summarises the results of the circular uniformity tests. % UA3c – Mean
 416 direction: 77.17° (E), circular variance: 41.95° ; Mean dip: 20.35° , variance: 4.36°
 417 With regard to the UA3c sample, the Rayleigh test (p -value = 0.029) rejected the null
 418 hypothesis of circular uniformity. The mean resultant length ($\bar{R} = 0.268$) and the mean

Table 3: Value and p – value of circular uniformity test statistics.

Sample	mean dir.	Rayleigh		Kuiper		Watson		Rao	
		R	p	V_n	p	U^2	p	U	p
UA3c	77.17°	0.268	0.029	2.4698	<0.01	0.2967	<0.01	271.8367	<0.001
UA4	35.79°	0.386	0.003	2.5656	<0.01	0.3437	<0.01	246.3158	<0.001
<i>E. (P.) antiquus</i>	54.64°	0.489	2.775e-07	3.4811	<0.01	0.906	<0.01	291.4286	<0.001
UB4c (clock)	83.96°	0.167	0.091	2.327	<0.01	0.2466	0.01 < p < 0.025	309.7674	<0.001
UB4c (compass)	128.14°	0.225	0.037	1.6917	0.05 < p < 0.10	0.1862	0.05 < p < 0.10	153.3846	0.01 < p < 0.05

419 direction of 77.17° are thus significant, assuming the distribution is unimodal. How-
 420 ever, the rose diagram (Fig. 5a) shows a multimodal distribution. The Kuiper, Watson
 421 and Rao omnibus tests, more powerful than the Rayleigh test in detecting multimodal
 422 deviation from uniformity, also rejected the null hypothesis of uniformity, therefore
 423 suggesting significant multimodal anisotropy in the distribution.

424 For the UA4 sample and the subset of elephant bones, all the tests agreed in reject-
 425 ing the null hypothesis in favour of a preferentially oriented distribution. The Elephant
 426 sample, with respect to the other, showed stronger anisotropy and significantly higher
 427 \bar{R} . As suggested by the rose diagrams (Fig. 5c), this sample has a mean direction to-
 428 wards the NE (55°) and relatively low circular variance (29°).

429 The UB4c sub-samples had discordant test results when considering the Rayleigh
 430 and the omnibus statistics. According to the Rayleigh test, the mean resultant length
 431 (\bar{R}) and the mean direction were not significant for the sub-sample of measurements
 432 recorded with the clock system. However, this sample does not respect the assump-
 433 tion of unimodality of the Rayleigh test (Fig. 5d). Conversely, a significant test result
 434 was obtained for the sub-sample of measurements recorded using the compass, which
 435 shows a normal (von Mises) distribution (Fig. 5e).

436 The results obtained for the UA3c sample and the UB4c sub-sample recorded using
 437 the clock method are most probably due to the shape of those distributions. Indeed, the
 438 clock system, being less accurate, tends to produce a less dense distribution, more
 439 subject to show a multimodal shape when the distribution is actually uniform (Fig. 5a,
 440 d).

441 The Woodcock eigenvalues ratio graph (Fig. 6a) presents the shape (K) and strength
 442 (C) of the distributions. Fig. 6b plots confidence levels of Monte-Carlo critical C val-
 443 ues, varying for sample sizes. The two samples from Area B, together with the UA3c
 444 sample, having low C values, plotted close to the origin of the ratio graph. Thus,
 445 they suggest weak preferential orientation (UA3c) and nearly significant randomness
 446 (UB4c). On the other hand, the UA4 and the elephant samples, with higher C values,
 447 showed a stronger and significant tendency to orient preferentially. The shape param-
 448 eter K of the samples varied from $K = 0.2$ for the UB4c sample measured with the
 449 compass, to $K = 0.6$ for the one measured with the clock, to $K = 5$ for the elephant
 450 sample. Overall, all the samples, except the UA3c one, plotted below the average shape
 451 value ($K = 1$) between girdles and clusters distributions.

452 The Benn diagram (Fig. 7) resembles the Woodcock ratio graph (Fig. 6a). The
 453 samples from units UB4c and UA3c clearly plotted at a distance from the UA4 and the
 454 elephant samples. The UB4c samples plotted in the upper corner of the ternary graph,
 455 with the UB4c sub-sample of measurements taken using the clock system exhibiting
 456 more isotropy. The UA3c sample, with an elongation index similar to the elephant

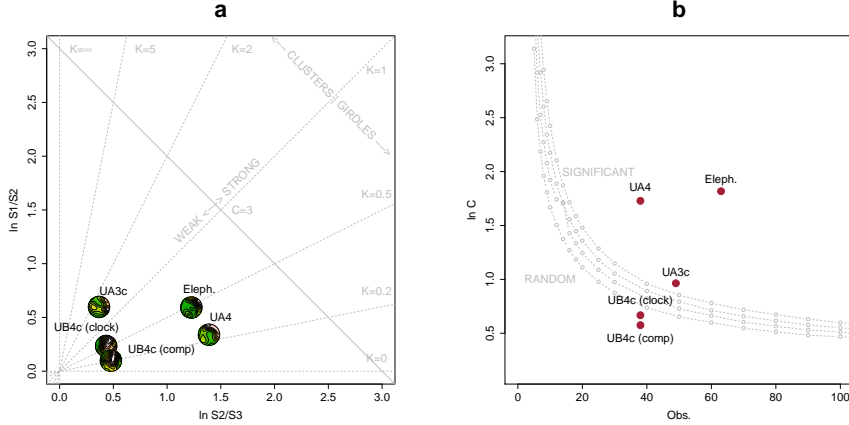


Figure 6: Woodcock's eigenvalues ratio graph (a) and plot of the Monte-Carlo critical S_1/S_3 test values, for varying sample sizes and confidence levels (b), modified from [Woodcock and Naylor \(1983\)](#).

457 sample, but higher isotropix index, plotted towards the centre.

458 Compared to the ranges recorded for modern natural processes (debris flow, runoff,
459 solifluction), the fabric from the UA3c and UB4c units plotted well inside the cluster of
460 debris flows, with the UB4c (clock) sample suggesting even more random orientations.
461 On the other hand, the sample of elephant remains, which lie mostly on UA4 and are
462 covered by UA3c, plotted significantly close to the sample from unit UA4. They both
463 presented the lowest isotropy index (IS), but not high elongation index (EL). Thus,
464 they plotted in the average between linear and planar orientations, within the range of
465 runoff processes. Yet they still plotted at the margins of the cluster of debris flows
466 fabrics. Moreover, the elephant sample showed a more linear attitude with respect to the
467 UA4 sample.

468 3.2. Vertical distribution

469 Fig. 8 compares the distribution of the absolute elevations of the partial skeleton
470 of the *Elephas (P.) antiquus* with the other remains from Area A. Overall, the vertical
471 distribution of the elephant approximates a normal distribution with mean (μ) 349.25 m
472 a.s.l. and standard deviation (σ) 0.12 m. The mean elevation of the erosional contact
473 between the two stratigraphic units is slightly above the latter ($\mu = 349.30$ m). Al-
474 though difficult to quantify due to its mixed nature, the range of elevations of this con-
475 tact, as estimated from the IDW interpolation (Fig. 8a), is relatively small ($\sigma = 0.06$ m).

476 Three lithic artefacts (two flakes and one tool) from the UA3c unit are located
477 within its positive half. Only one flake has been found in the lower UA4, at about
478 349.10 m, together with three chips. However, they plotted well within the left tail
479 of the debris/chip distribution from the unit above. Despite the scarcity ofdebitage
480 products in this area, waste products (debris/chip) are relatively well represented (16%
481 of the UA3c sample). Their vertical distribution approximates a normal distribution
482 ($\mu = 349.50$ m and $\sigma = 0.18$ m), having almost 50% of the sample in the range of

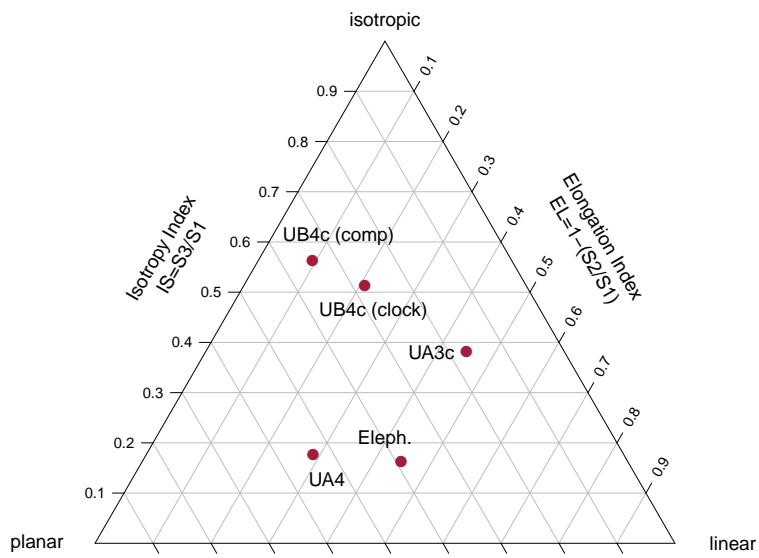


Figure 7: Benn's diagram. Fabric ranges of natural processes modified from Bertran et al. (1997); Lenoble and Bertran (2004).

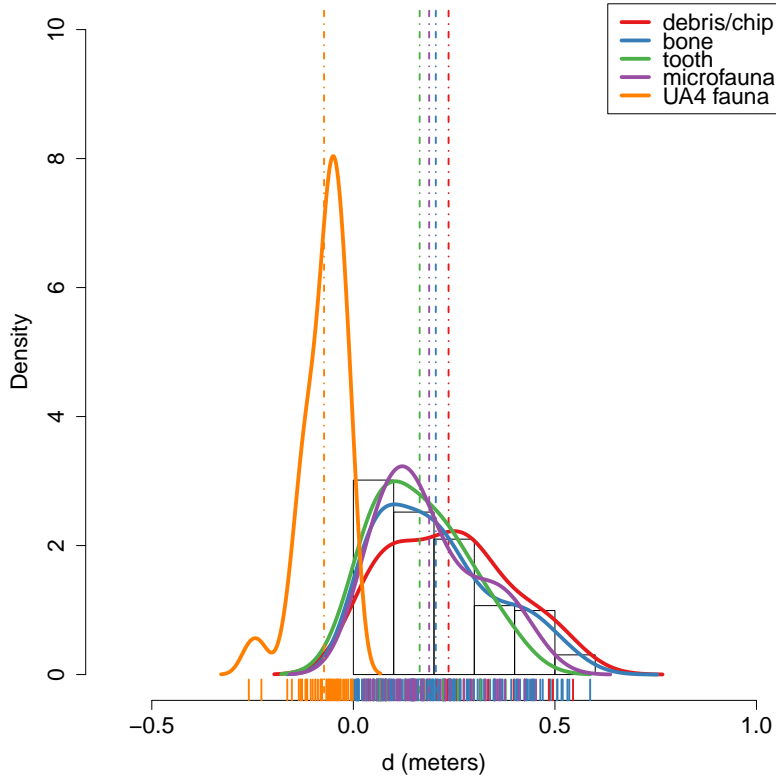


Figure 8: Empirical density functions of absolute elevations (meters a.s.l) of remains from Area A. The histogram represents the *Elephas (P.) antiquus* range of elevations; the grey area shades the $Q_3 - Q_1$ range of the erosional UA3c/4 surface; dashed lines indicate mean values.

elevations of the erosional surface and the rest above it. Notably, the distribution of the faunal remains from the same unit resembles that of the debris/chip. The Welch two sample t-test ($p - value = 0.5099$) failed to reject the null hypothesis that the two population means are equal. On the other hand, the vertical distribution of faunal remains recovered from the UA4 unit is comparable with that of the *Elephas* ($p - value = 0.6562$). Nevertheless, the density functions altogether clearly confirm one of the main observations assessed during excavation, namely that the elephant remains and most of the recovered faunal and lithic material in Area A lie at or close to the UA3c/4 contact, with unit UA3c covering the remains.

Fig. 9 shows the empirical density functions of the minimum distances from each specimen from Area B to the UB4c/5a erosional contact (Fig. 4b). The combined distribution of any type of find from the UB5a unit (Fig. 9a) skewed to the left with

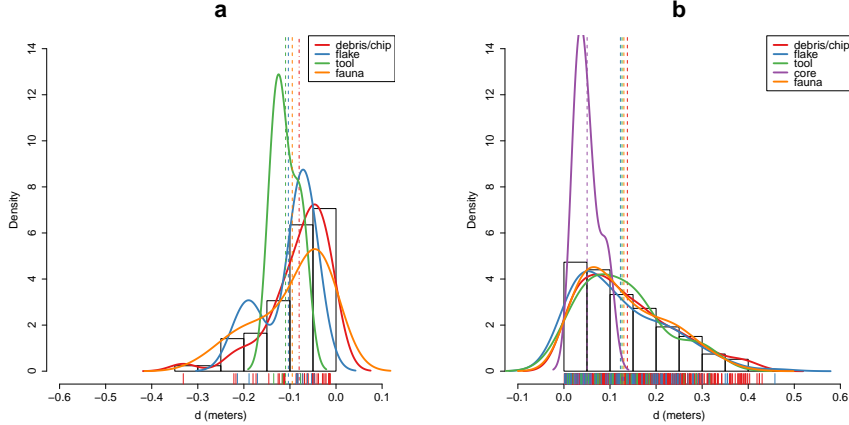


Figure 9: Empirical density functions of minimum orthogonal distances (d) to the UB4c/5a surface. The histogram represents the total distribution of remains from UB5a (a) and UB4c (b); dashed lines indicate mean values.

a short tail (up to -0.3 m). The mode, between 5 and 10 cm below the roof of UB5a, indicates a general concentration of material very close to the contact of this unit with the overlying UB4c, in accordance with the mean distribution of the different classes of remains. Although the majority of both the lithic and faunal assemblages were found in the uppermost 15 cm of UB5a, few debris/chips and bone fragments occur lower in the sequence, yet no more than 30 cm below the roof of this unit. Very few flakes, three tools and no cores have been found in this unit. As a whole, the lithic assemblage from UB5a, mostly composed by debris/chips, is only 7% of the most conspicuous assemblage from UB4c.

The global distribution of unit UB4c was right skewed (up to almost 0.6 m) and centred at about 5 cm above the contact with the underlying unit UB5a (Fig. 9b). Almost 30% of the sample fell exactly at the erosional contact that separates UB4c from UB5a. The density estimations of the lithic debris/chip, flakes, tools and faunal remains significantly overlap, whereas the distribution of the six cores shows a bimodal shape with peaks at 5 and 20 cm above the contact. However, the Welch Two Sample t-test of the lithic and faunal sample means failed to reject the null hypothesis ($p-value = 0.6295$).

3.3. Point pattern analysis

Results of the point pattern analysis are complementary to those obtained from the analysis of the vertical and fabric distributions.

Regarding Area A, kernel density estimation and three-dimensional functions were applied in order to quantitatively depict the spatial distribution of the lithic assemblage in relation to the elephant skeleton.

Fig. 10a shows the smoothing kernel intensity estimation of the faunal assemblage from the UA3c unit. Contour lines delimit the density of the lithic sample. The partial skeleton of the *E. (P.) antiquus* is superimposed on it. A preliminary visual examination

of the plot suggests a homogeneous distribution of lithics (mostly debris/chips) and fossils. Spots of higher density appear to be spread around and in association with the elephant remains.

The univariate pair correlation function of the joined lithic assemblage from the UA3c and UA4 units (Fig. 10b) suggests aggregation of finds. The estimated $\hat{g}_3(r)$ function (black solid line) wanders above the benchmark value (red dotted line) until values of $r = 0.8$. However, for distances between 35 and 65 cm, it lies above the grey envelope of significance for the null hypothesis of CSR, indicating that at those distances artefacts occur closer than expected in the case of random processes. For values of $r > 0.8$, the function stabilises at values close to 0, suggesting a Poisson distribution. The plot illustrates the random distribution of finds between patches of clusters that we observe in the kernel density estimation (Fig. 10a).

The histogram in Fig. 10c shows the density of the distances calculated from each artefact to the nearest-neighbour elephant remain. A right skewed distribution, with a prevalent peak at 10 cm and mean $\mu = 30$ cm is an indication of the relatively strong aggregation of events around the mass of the elephant skeleton.

As for Area B, the analysis first focused on the spatial distribution and cross-correlation of the assemblages from UB4c and UB5a (Fig. 11); and secondly on the interaction between classes of remains from UB4c (Fig. 12).

Figs. 11a,b respectively show kernel density estimations of the combined lithic and faunal assemblages from both the units analysed. Despite the samples size difference, a first visual examination suggests the presence of interesting spatial structures.

Regarding the UB4c unit (Fig. 11a), the high density of material concentrated around the western square 934/600 suggests that the pattern could have been the result of an inhomogeneous, non-uniform depositional process. Visual comparison of the density plot with the elevation model of the erosional contact between the UB4c and UB5a units (Fig. 4b) suggests positive correlation between lower elevations (topographic depressions) and higher density of remains. Fig. 11c shows the results of the ρ -function, which estimates the intensity of the UB4c sample assemblage as a function of the covariate underlying topography created by the erosional event. Within the range of elevation between 350.2 and 350.4 m, the occurrence of finds is higher and the intensity decreases with the rise of elevation, i.e., finds are more likely to be found at lower elevations than would be expected if the intensity was constant.

Spatial Kolmogorov-Smirnov and Berman's Z_2 (Berman, 1986) statistics were used in order to test the dependence of the UB4c pattern on the covariate erosional surface. Both KS ($D = 0.11952$, $p - \text{value} = 7.772e - 16$) and Z_2 ($Z_2 = -7.8447$, $p - \text{value} = 4.34e - 15$) significantly rejected the null hypothesis of CSR. Although the tests suggested evidence that the intensity depends on the covariate, the effect of the covariate is weak and it seems to have no discriminatory power. The ROC curve and AUC statistics (0.56), which measure the strength of the covariate effect, suggest that the underlying UB4c/5a topography does not completely explain the localised high density of occurrence in the UB4c.

Relative spatial segregation seems to occur between the assemblages from UB4c (Fig. 11a) and UB5a (Fig. 11b), with high density of the former distribution corresponding to low density of the latter. The former analysis of the vertical distribution showed that the two assemblages occur very close to their stratigraphic contact. In

.../artwork/Fig11-eps-converted-to.pdf

Figure 10: Kernel smoothed intensity function of the lithic and faunal assemblages from UA3c. Isolines mark the density of the lithic artefacts (a). Pair correlation function ($g_3(r)$) of a three-dimensional pattern of lithic artefacts from UA3c and UA4. Grey envelope of 999 Monte Carlo simulations under the CSR null hypothesis (b). Three-dimensional distance from each lithic artefact from UA3c and UA4 to the nearest neighbour elephant remain (c).

order to further investigate the spatial interaction between the two depositional events, we applied multitype pair correlation ($g_{ij}(r)$) and nearest-neighbour ($G_{ij}(r)$) functions.

Fig. 11d shows the estimated values of the multivariate $\hat{g}_{ij}(r)$ function against the envelope of the null hypothesis, obtained by randomly shifting the position of remains from the two distributions in 199 Monte Carlo simulations. For fixed values of r less than 30 cm the observed function lies below the benchmark value of independence, thus indicating segregation; but it wanders at the lower edge of the grey envelope. For fixed distances of $r > 0.3$ m the observed and theoretical lines significantly overlap. Overall, the function suggests independence of the two point processes (UB4c and UB5a) at multiple scales.

However, the estimated $\hat{G}_{ij}(r)$ function (Fig. 11c), running well below the significance grey envelope for fixed values of $r > 0.3$ m, confirms that the nearest-neighbour distances between remains from UB4c and UB5a are significantly longer than expected in the case of independent processes. Interestingly, at values of $r < 0.2$ m the observed function failed to reject the null hypothesis of Complete Spatial Randomness and Independence (CSRI).

With the aim to integrate the vertical distribution analysis, the particle size spatial distribution of remains from the UB4c unit were investigated by means of a derivative of the multitype K -function, randomly labelling the classes of remains. Fig. 12 shows a selection of the array of possible combinations between classes. In any panel, the estimated function wanders above the benchmark value. Such positive deviations from the null hypotheses suggest that debris/chips are more likely to be found close to the other class of remains than would be expected in case of a completely random distribution. Permutating the lithic debris/chips with flakes (Fig. 12a), tools (Fig. 12b), cores (Fig. 12c) and faunal remains (Fig. 12d), the Monte Carlo test results would have been significantly consistent with clustering, if we had chosen distance values $r > 0.4$, $r > 0.4$, $r > 0.9$, $r > 0.8$, respectively. Conversely, we could not reject the null hypothesis of CSRI for lesser values of r .

4. Discussion

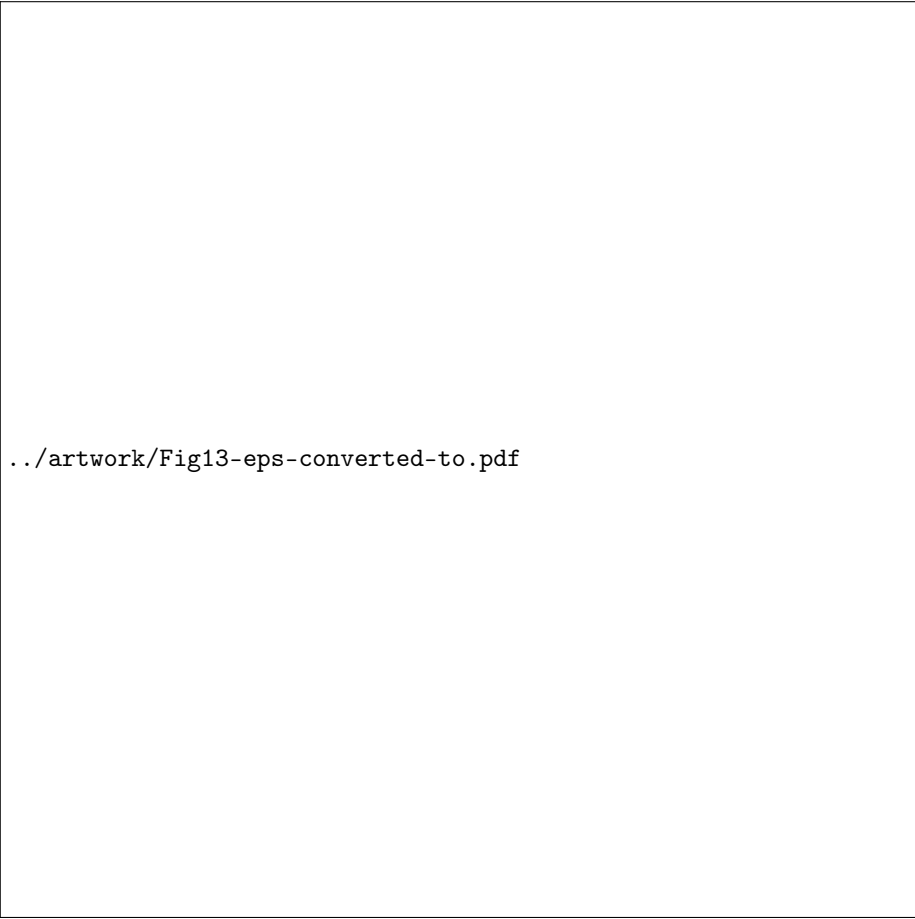
Recent excavations at the Middle Pleistocene site of Marathousa 1 have unearthed in one of the two investigated areas (Area A) a partial skeleton of a single individual of *Elephas (P.) antiquus*, whose bones are in close anatomical association, and spatially and stratigraphically associated with lithic artefacts and other faunal remains. In Area B, 60 m to the South of Area A, we collected a much higher number of lithic artefacts (Tourloukis et al., this issue), spatially and stratigraphically associated with other faunal remains, including isolated elephant bones, cervids and carnivores among others (Konidaris et al., this issue).

The two areas are stratigraphically correlated, the main fossiliferous layers (UA3c and UB4c) representing a massive depositional process, such as a hyperconcentrated flow that dumped material in a lake margin context (Karkanas et al., this issue).

To date, evidence of butchering (cut-marks) has been identified on two bones of the elephant skeleton from Area A, as well on elephant and other mammal bones from Area B (see Konidaris, this issue).

.../artwork/Fig12-eps-converted-to.pdf

Figure 11: Kernel smoothed intensity function of the lithic and faunal assemblages from UB4c (a) and UB5a (b). Smoothing estimate of the intensity of remains from UB4c, as a function of the erosional surface UB4c/5a. Grey shading is pointwise 95% confidence bands (c). Cross-pattern pair correlation function ($g_{ij}(r)$) between the UB4c and UB5a distributions. Grey envelope of 199 Monte Carlo simulations under the independence of components null hypothesis (d). Multitype nearest-neighbour function ($G_{ij}(r)$) between the UB4c and UB5a distributions (e).



./artwork/Fig13-eps-converted-to.pdf

Figure 12: Random labelling test for the UB4c assemblage. Grey pointwise envelope of 199 Monte Carlo permutation of debris/chips with flakes (a); tools (b); cores (c); fossils (d).

609 However, due to the secondary depositional nature of the main fossiliferous horizon,
610 it is of primary importance to evaluate the degree and reliability of the spatial
611 association of the lithic artefacts with the faunal remains, and especially with the ele-
612 phant skeleton. In order to tackle our main objective, we applied a comprehensive
613 set of spatial statistics to the distributions of the archaeological and zooarchaeologi-
614 cal/palaeontological remains from relevant stratigraphic units of the two areas of in-
615 vestigation. Preliminary results of our analyses are here discussed for both areas.

616 *4.1. Fabric analysis*

617 The analysis of the orientation (dip and strike) of subsets of remains, mostly bone
618 fragments, organic residues and lithic artefacts, showed different patterns for the two
619 main find-bearing units.

620 The test results (Tab. 3) for the UA4 sample and the sample of elephant remains
621 - which lie on unit UA4 and are covered by UA3c - indicated significant preferential
622 orientations towards the NE (Figs. 5b,c). As shown by the Woodcock's (Fig. 6) and the
623 Benn's diagrams (Fig. 7), these samples plotted together at a distance from the others.
624 Such convergence suggests that the elephant carcass, the other faunal remains and the
625 organic material, deposited on unit UA4, were subject to the same processes.

626 Far from the isotropic corner in the Benn's diagram these two samples from Area
627 A plotted approximately in between the linear and planar extremes, with the elephant
628 sample showing a more planar fabric. When the results published by Bertran et al.
629 (1997) and Lenoble and Bertran (2004) from observations of fabrics in modern sub-
630 aereal slope deposits were used as a reference, the two samples aggregated well within
631 the cluster of runoff process. Yet, they still plotted at the extreme margins of debris
632 flow and relatively distant from the linear corner.

633 This result is consistent with the exposure of unit UA4 to overland water-laden
634 processes that occurred before the flood event UA3/UB4 (Karkanas et al., this is-
635 sue). Notably, the erosive nature of low-energy processes triggered by rain-water has
636 been observed on lacustrine floodplains, and is associated with anisotropic patterns
637 in autochthonous assemblages (Cobo-Sánchez et al., 2014; Domínguez-Rodrigo et al.,
638 2014c; García-Moreno et al., 2016).

639 On the other hand, the fabric of the UA3c sample, being similar to those of the
640 UB4c sub-samples (Figs. 6 and 7), supports the stratigraphic correlation between these
641 units across the two investigated areas. The fabric analysis suggests that the UA3/UB4
642 process can be categorized as a flood event, which falls in between the spectrum of de-
643 bris and hyperconcentrated flow. Indeed, random distribution and orientation of clasts
644 is expected for debris flows, except at flow margins, where preferential orientation and
645 clusters of clasts have been observed (Pierson, 2005).

646 Unlike bones with a tubular shape (i.e., long bones), ribs and vertebrae are prone
647 to orient preferentially under high energy processes, less likely under low energy pro-
648 cesses (Domínguez-Rodrigo and García-Pérez, 2013; Domínguez-Rodrigo et al., 2014c).
649 Interestingly, whereas some of the ribs share the same preferential orientation with the
650 long bones, others are oriented NW/SE. However, a NW/SE orientation could be con-
651 sistent with a prevalent NE direction of the flow (and vice-versa), since long bones
652 could roll orthogonally to the flow direction (Voorhies, 1966).

653 On the other hand, a higher energy flood would lead to an under-representation
654 of most cancellous grease-bearing bones, which are prone to be easily transported by
655 water induced processes (Voorhies, 1966). Yet several carpals, tarsals, metapodials,
656 phalanges, ribs and vertebrae are present and in close spatial association with the ele-
657 phant cranium and other skeletal elements.

658 The presence of many of the skeletal elements suggests that the elephant carcass
659 was not subjected to high energy processes. Thus, we can assume that relatively low
660 energy overland flows slightly reworked and oriented the exposed elements of the
661 already dismembered (and probably already marginally displaced) elephant carcass,
662 which mostly preserves close anatomical associations, but not anatomical connections.

663 In Area B, two sub-samples from the same stratigraphic unit were analysed, accord-
664 ing to the different methods used for recording the orientation (dip and strike) of the
665 finds (i.e., 'clock' vs. compass), mostly faunal remains, wood fragments and lithic arte-
666 facts. Due to the different shapes of the two distributions (Figs. 5d,e), test statistics re-
667 ported contrasting results (Tab. 3). Indeed, the clock system, recording non-continuous
668 circular data, tends to produce a distribution more subject to show a multimodal shape
669 when the distribution is actually uniform. However, the three-dimensional Woodcock
670 (Fig. 6) and Benn (Fig. 7) diagrams agreed upon assessing the randomness of the sam-
671 ples. Despite minor differences between the two samples, both plotted with the UA3c
672 sample in the reference range of debris flows.

673 4.2. Vertical distribution

674 As for the vertical distribution, we assume that mass wasting processes, such as
675 debris or hyperconcentrated flows, would predominantly distribute extremely poorly
676 sorted clasts homogeneously throughout the sequence. Normal or inverse grading can
677 be observed in such flows (Pierson, 2005). A concentration of unsorted elements in the
678 proximity of the erosional surface, as well as the absence of any grading, would in turn
679 suggest an autochthonous assemblage.

680 The lithic assemblage from Area A - the combined sample from units UA3c and
681 UA4 ($n = 54$), composed by a fewdebitage products and a relatively high number of
682 debris/chips and retouch waste products (Tab. 2) - plotted predominantly in the prox-
683 imity of the erosional surface created by the UA3/UB4 event. The faunal remains
684 from unit UA3c resemble the distribution of the archaeological assemblage as a whole;
685 whereas the ones from the underlying unit UA4 match the vertical distribution of the
686 elephant (Fig. 8).

687 Overall, the material recovered from unit UA3c did not show any grading and
688 mainly plotted at the bottom of the unit, thus is consistent with the hypothesis of an
689 autochthonous assemblage.

690 In Area B, two samples from units UB4c ($n = 1243$) and UB5a ($n = 101$) respec-
691 tively, were analysed (Tab. 2) for quantifying the minimum orthogonal distance of each
692 item to the modelled erosional surface (Fig. 4b).

693 The vertical distribution of lithic artefacts and fossils from unit UB4c showed a pre-
694 dominant peak right at the contact with the erosional surface. Almost 30% of this rich
695 sample plotted at a distance between 0 and 5 cm from the erosional contact; whereas
696 the rest gently skewed to the upper part of the unit, up to about 50 cm. The same distri-

697 bution was observed for all classes of remains, suggesting no size sorting and an origin
698 very close to the erosional surface (Fig. 9b).

699 The density distribution of the sample from the underlying UB5a unit (Fig. 9a)
700 globally indicates a more constrained vertical displacement of remains (within 30 cm
701 below the erosional surface). Whereas lithic artefacts and fossils mostly plot right at
702 the contact and just below it, a few debris/chips and faunal remains were found lower
703 in the sequence. No size sorting was observed, but, notably, lithic cores are absent and
704 the debris/chip distribution is wider than the distribution of the few flakes and tools.

705 Field observations of cracks in the clayey UB5a unit testify to shrinking and swelling
706 during wet and dry cycles (Karkanas et al., this issue), which suggests that vertical dis-
707 placement of some small lithics and fossil fragments at lower depths with respect to
708 the UB5a/4c contact probably resulted from clay desiccation.

709 Likewise, [Lenoble and Bertran \(2004\)](#) documented up to 30 cm vertical dispersion
710 and frequent vertical dip of artefacts from the marshy silty clay of the Croix-de-Canard
711 site, sector 3.

712 Furthermore, a recent experimental study of animal trampling in water saturated
713 substrates reported negative correlation with artefact size, significant inclination and
714 greater vertical displacement than any former work: a maximum between 16 and
715 21 cm, with a mean of about 6 cm ([Eren et al., 2010](#)).

716 The fact that the majority of the remains from units UB4c and UB5a plotted at,
717 or very close to the contact between these two layers, the relatively high percentage
718 of lithics in both units, as well as the absence of size sorting or grading, suggest au-
719 tochthonous assemblages, deposited in UB5a and subsequently eroded *in situ* by the
720 UA3/UB4 flood event.

721 4.3. Point pattern analysis

722 The hypothesis that in both areas the lithic and faunal assemblages were primarily
723 deposited *in situ* and were subsequently reworked by a low energy flood, was further
724 explored by means of point pattern analysis.

725 We assumed that a completely random spatial distribution of the lithic artefacts
726 and faunal remains would suggest an allochthonous origin and subsequent transport to
727 the site by the action of a random massive process, such as debris flow. Nevertheless,
728 clustering of artefacts is not necessarily evidence of human presence. Aggregation or
729 segregation patterns could be produced by a range of biotic and/or natural processes.
730 Human activities, topography and physical obstructions alike could trigger spatial ag-
731 gregation.

732 The three-dimensional distribution of lithic artefacts from unit UA3c shows signif-
733 icant clustering for values of r between 35 and 65 cm. Lithic artefacts occur relatively
734 close to the skeletal elements of the elephant, at a distance between 20 and 50 cm at
735 most (Fig. 10). The richest cluster of about 20 lithic artefacts is located to the SW of
736 the cranium, close to the right femur and the scatter of ribs and vertebrae.

737 Considering the prevalent NE orientation of the elephant bones and the other fau-
738 nal remains from UA4, it is not unlikely that a SW/NE oriented flood could have been
739 responsible for the observed accumulation to the SW of the elephant cranium, which
740 would have represented an important obstruction to the flow. A similar case of clus-
741 tering of small remains, apparently dammed by a long elephant tusk, has also been

742 observed at Castel di Guido (Italy) ([Boschian and Saccà, 2010](#)). Secondary deposition
743 by low-energy flows and clustering of artefacts and bones blocked by an aurochs
744 carcass have been as well documented at the site of 'Ein Qashishadd (Israel) ([Hovers
745 et al., 2014](#)).

746 As mentioned above, whereas fairly random fabric and spatial distribution of coarse
747 clasts are observed at the centre of modern debris flow deposits, preferential orientation
748 and clustering may occur at the margin of the flood ([Pierson, 2005](#)). Yet the fabric
749 analysis of the UA3c sample shows a random distribution, which falls within the range
750 of debris flow (Fig. 7), and the pair correlation function (Fig. 8b) suggests significant
751 clustering of lithic artefacts at relatively small scale: a pattern less likely to be produced
752 by a large scale massive process such as a debris flow. Moreover, clusters of lithic
753 artefacts occur as well in areas with lower densities of elephant bones.

754 Small scale clustering; proximity to the elephant remains and the erosional surface;
755 absence of spatial size sorting and, on the contrary, the presence of a relatively high
756 number of lithic debris/chips associated with some flakes and tools; close anatomical
757 spatial association of the elephant skeletal elements, slightly displaced and preferen-
758 tially oriented: these lines of evidences support the hypothesis of an autochthonous
759 deposition, subject to localised minor reworking.

760 A similar pattern can be observed in Area B, where an initial set of spatial statistics
761 confirmed that the inhomogeneous density of remains from unit UB4c (Fig. 11a) is
762 not completely explained by the covariate effect of the underlying complex topography
763 created by the erosional event UA3/UB4 (Fig. 4b).

764 Thus, we explored the relative spatial interaction between the UB4c and the un-
765 derlying UB5a samples. We assumed that complete spatial randomness of the two
766 independent depositional processes would occur in case of an exogenous origin and
767 transportation of the UB4c assemblage. The hypothesis of an autochthonous original
768 deposition of the faunal and lithic assemblages on the UB5a unit, subsequently eroded
769 *in situ* by a relatively high energy flood (UB4c), was tested by cross-pattern spatial
770 correlation functions (Figs. 11d,e). Whereas the two samples are vertically adjacent to
771 the erosional surface (Fig. 9), on the horizontal plane they are both more segregated
772 than expected for a random distribution.

773 Moreover, for the UB4c sample, an unsorted particle size spatial distribution was
774 confirmed (Fig. 12). The occurrence in the same place of small and large classes of
775 remains suggests that post-depositional processes, such as water winnowing, have not
776 severely affected the assemblage. Hyperconcentrated flows would have dumped mate-
777 rial onto the lake margin. In this way, particles would have been frozen and deposited
778 *en masse*. Hence their non-sorted spatial distribution.

779 Conversely, the extraordinary preservation and number of mint to sharp, unsorted
780 lithic artefacts from the UB4c unit; their density, positively correlated to the topog-
781 raphy, and significantly segregated from the underlying distribution of remains; the
782 vertical proximity of both assemblages from UB4c and UB5a to the erosional surface;
783 as well as the random orientation pattern of the former, suggest that significant dis-
784 placement of materials due to the erosional event can be excluded.

785 The faunal and lithic assemblages from unit UB4c therefore most likely derived
786 from the local erosion of exposed mudflat areas (UB5a layer) and have been slightly
787 redistributed by the same flood event that capped the elephant in Area A.

788 Further evidence that the recovered assemblage has not undergone substantial re-
789 working and has retained its original characteristics would come from the refitting anal-
790 ysis, currently in progress. To date, 4 bone refits have been found in Area B: three from
791 unit UB4c, respectively at 4.77, 0.05 and 0.01 m distance; and one between two mam-
792 mal bone fragments from units UB4c and UB5a, at a very short distance (0.09 m).
793 Interestingly, one of the elements of the most distant refit (a *Dama sp.* mandibular
794 fragment) shows traces of carnivore gnawing (Konidaris et al., this issue).

795 In conclusion, multiple lines of evidence suggest that the erosional event UB4/UA3
796 represents a relatively low-energy process in the continuum between debris and hyper-
797 concentrated flow, which would have locally reworked at a small scale the already
798 exposed or slightly buried and spatially associated lithic and faunal assemblages.

799 Although the UB4/UA3 process represents a snapshot of a relatively short time-
800 frame, inferences about the use of space by human groups, in terms of knapping
801 episodes and butchering activities, are unreliable in light of the current information.

802 The spatial pattern observed at the site is indeed the result of the last episode in
803 a palimpsest of spatial processes. Whereas the erosional event represented by the de-
804 bris/hyperconcentrated flow UA3/UB4 caps the sequence and preserves the record, lit-
805 tle is known about the eroded underlying occupational horizon.

806 However, whereas hunting or scavenging is still an unsolved matter of debate, con-
807 sidering the rate of bone fragmentation, the density of lithic debris/chips, the number
808 of processed bones and their spatial density and association, it is likely that the assem-
809 blage represents a complex palimpsest of locally repeated events of hunting/scavenging
810 and exploitation of lake shore resources.

811 More data from high resolution excavations in the coming years will allow us to
812 refine the coarse-grained spatio-temporal resolution of our inferences about past human
813 behaviour at Marathousa 1.

814 5. Conclusions

815 At the Middle Pleistocene open-air site of Marathousa 1, a partial skeleton of a
816 single individual of *Elephas (Palaeoloxodon) antiquus* was recovered in stratigraphic
817 association with a rich and consistent lithic assemblage and other vertebrate remains.
818 Cut-marks and percussion marks have been identified on the elephant and other mam-
819 mal bones excavated at the site. The main find-bearing horizon represents a secondary
820 depositional process in a lake margin context.

821 Understanding the site formation processes is of primary importance in order to
822 reliably infer hominin exploitation of the elephant carcass and other animals. To meet
823 this aim, we applied a comprehensive set of multivariate and multiscale spatial analyses
824 in a taphonomic framework.

825 Results from the fabric, vertical distribution and point pattern analyses are consis-
826 tent with a relatively low-energy erosional process slightly reworking at a small scale
827 an exposed (or slightly buried) and consistent scatter of lithic artefacts and faunal re-
828 mains. These results are in agreement with preliminary taphonomic observations of
829 the lithic artefacts (Tourloukis et al., this issue) and the faunal remains (Konidaris et
830 al., this issue), which also indicate minor weathering and transportation. Our analyses

831 show that multiple lines of evidence support an autochthonous origin of the lithic and
832 faunal assemblages, subject to minor post-depositional reworking. Human activities
833 therefore took place on-site, during an as of yet uncertain range of time.

834 **Acknowledgements**

835 This research is supported by the European Research Council (ERC StG PaGE
836 283503) awarded to K. Harvati. We are grateful to the Municipality of Megalopolis,
837 the authorities of the Region of Peloponnese, and the Greek Public Power corporation
838 (Δ EH) for their support. We also thank Julian Bega and all the participants in the PaGE
839 survey and excavation campaigns in Megalopolis for their indispensable cooperation.

840 **References**

- 841 Anderson, K. L., Burke, A., 2008. Refining the definition of cultural levels at Karabi
842 Tamchin: a quantitative approach to vertical intra-site spatial analysis. *Journal of
843 Archaeological Science* 35 (8), 2274–2285.
- 844 Baddeley, A., Chang, Y.-M., Song, Y., Turner, R., 2012. Nonparametric estimation of
845 the dependence of a point process on spatial covariates. *Statistics and Its Interface*
846 5 (2), 221–236.
- 847 Baddeley, A., Rubak, E., Turner, R., 2015. *Spatial Point Patterns: Methodology and
848 Applications* with R. Chapman and Hall/CRC, London.
- 849 Bailey, G., 2007. Time perspectives, palimpsests and the archaeology of time. *Journal
850 of Anthropological Archaeology* 26 (2), 198 – 223.
851 URL [http://www.sciencedirect.com/science/article/pii/
852 S0278416506000481](http://www.sciencedirect.com/science/article/pii/S0278416506000481)
- 853 Bar-Yosef, O., Tchernov, E., 1972. On the palaeo-ecological history of the site of Ubei-
854 diya. Vol. 35. Israel Academy of Sciences and Humanities, Jerusalem.
- 855 Bargalló, A., Gabucio, M. J., Rivals, F., 2016. Puzzling out a palimpsest: Testing
856 an interdisciplinary study in level o of abric romani. *Quaternary International*
857 417 (Supplement C), 51 – 65, advances in Palimpsest Dissection.
858 URL [http://www.sciencedirect.com/science/article/pii/
859 S1040618215009635](http://www.sciencedirect.com/science/article/pii/S1040618215009635)
- 860 Benito-Calvo, A., de la Torre, I., 2011. Analysis of orientation patterns in Olduvai
861 Bed I assemblages using GIS techniques: Implications for site formation processes.
862 *Journal of Human Evolution* 61 (1), 50 – 60.
- 863 Benito-Calvo, A., Martínez-Moreno, J., Mora, R., Roy, M., Roda, X., 2011. Trampling
864 experiments at Cova Gran de Santa Linya, Pre-Pyrenees, Spain: their relevance for
865 archaeological fabrics of the Upper–Middle Paleolithic assemblages. *Journal of Ar-
866 chaeological Science* 38 (12), 3652–3661.

- 867 Benito-Calvo, A., Martínez-Moreno, J., Pardo, J. F. J., de la Torre, I., Torcal, R. M.,
868 2009. Sedimentological and archaeological fabrics in Palaeolithic levels of the
869 South-Eastern Pyrenees: Cova Gran and Roca dels Bous Sites (Lleida, Spain). Journal
870 of Archaeological Science 36 (11), 2566 – 2577.
- 871 Benn, D., 1994. Fabric shape and the interpretation of sedimentary fabric data. Journal
872 of Sedimentary Research 64 (4a), 910–915.
- 873 Berman, M., 1986. Testing for spatial association between a point process and another
874 stochastic process. Applied Statistics 35, 54–62.
- 875 Bernatchez, J. A., 2010. Taphonomic implications of orientation of plotted finds from
876 Pinnacle Point 13B (Mossel Bay, Western Cape Province, South Africa). Journal of
877 Human Evolution 59 (3–4), 274 – 288.
- 878 Bertran, P., Hetù, B., Texier, J.-P., Steijn, H. V., 1997. Fabric characteristics of subaerial
879 slope deposits. Sedimentology 44 (1), 1 – 16.
- 880 Bertran, P., Texier, J.-P., 1995. Fabric Analysis: Application to Paleolithic Sites. Journal
881 of Archaeological Science 22 (4), 521 – 535.
- 882 Bevan, A., Crema, E., Li, X., Palmisano, A., 2013. Intensities, Interactions, and Un-
883 certainties: Some New Approaches to Archaeological Distributions. In: Bevan, A.,
884 Lake, M. (Eds.), Computational Approaches to Archaeological Spaces. Left Coast
885 Press, Walnut Creek, pp. 27–52.
- 886 Boschian, G., Saccà, D., 2010. Ambiguities in human and elephant interactions? Sto-
887 ries of bones, sand and water from Castel di Guido (Italy). Quaternary International
888 214 (1–2), 3 – 16.
- 889 Brantingham, P. J., Surovell, T. A., Waguespack, N. M., 2007. Modeling post-
890 depositional mixing of archaeological deposits. Journal of Anthropological
891 Archaeology 26 (4), 517 – 540.
892 URL [http://www.sciencedirect.com/science/article/pii/
893 S0278416507000359](http://www.sciencedirect.com/science/article/pii/S0278416507000359)
- 894 Carrer, F., 2015. Interpreting Intra-site Spatial Patterns in Seasonal Contexts: an Eth-
895 noarchaeological Case Study from the Western Alps. Journal of Archaeological
896 Method and Theory, 1–25.
- 897 Cobo-Sánchez, L., Aramendi, J., Domínguez-Rodrigo, M., 2014. Orientation patterns
898 of wildebeest bones on the lake Masek floodplain (Serengeti, Tanzania) and their
899 relevance to interpret anisotropy in the Olduvai lacustrine floodplain. Quaternary
900 International 322–323 (0), 277 – 284.
- 901 de la Torre, I., Benito-Calvo, A., 2013. Application of GIS methods to retrieve ori-
902 entation patterns from imagery; a case study from Beds I and II, Olduvai Gorge
903 (Tanzania). Journal of Archaeological Science 40 (5), 2446–2457.

- 904 Diggle, P., 1985. A kernel method for smoothing point process data. *Applied Statistics*
905 (Journal of the Royal Statistical Society, Series C) 34, 138–147.
- 906 Domínguez-Rodrigo, M., Bunn, H., Mabulla, A., Baquedano, E., Uribelarrea, D.,
907 Pérez-González, A., Gidna, A., Yravedra, J., Diez-Martin, F., Egeland, C., Barba,
908 R., Arriaza, M., Organista, E., Ansón, M., 2014a. On meat eating and human evolution:
909 A taphonomic analysis of BK4b (Upper Bed II, Olduvai Gorge, Tanzania), and
910 its bearing on hominin megafaunal consumption. *Quaternary International* 322–323,
911 129–152.
- 912 Domínguez-Rodrigo, M., Bunn, H., Pickering, T., Mabulla, A., Musiba, C., Baque-
913 dano, E., Ashley, G., Diez-Martin, F., Santonja, M., Uribelarrea, D., Barba, R.,
914 Yravedra, J., Carboni, D., Arriaza, C., Gidna, A., 2012. Autochthony and orientation
915 patterns in Olduvai Bed I: a re-examination of the status of post-depositional biasing
916 of archaeological assemblages from FLK North (FLKN). *Journal of Archaeological
917 Science* 39 (7), 2116 – 2127.
- 918 Domínguez-Rodrigo, M., Cobo-Sánchez, L., Yravedra, J., Uribelarrea, D., Arriaza, C.,
919 Organista, E., Baquedano, E., 2017. Fluvial spatial taphonomy: a new method for the
920 study of post-depositional processes. *Archaeological and Anthropological Sciences*,
921 1–21.
- 922 Domínguez-Rodrigo, M., Diez-Martín, F., Yravedra, J., Barba, R., Mabulla, A., Baque-
923 dano, E., Uribelarrea, D., Sánchez, P., Eren, M. I., 2014b. Study of the SHK Main
924 Site faunal assemblage, Olduvai Gorge, Tanzania: Implications for Bed II tapho-
925 nomy, paleoecology, and hominin utilization of megafauna. *Quaternary International*
926 322–323, 153–166.
- 927 Domínguez-Rodrigo, M., García-Pérez, A., 07 2013. Testing the Accuracy of Different
928 A-Axis Types for Measuring the Orientation of Bones in the Archaeological and
929 Paleontological Record. *PLoS ONE* 8 (7), e68955.
- 930 Domínguez-Rodrigo, M., Uribelarrea, D., Santonja, M., Bunn, H., García-Pérez, A.,
931 Pérez-González, A., Panera, J., Rubio-Jara, S., Mabulla, A., Baquedano, E., Yrave-
932 dra, J., Diez-Martín, F., 2014c. Autochthonous anisotropy of archaeological mate-
933 rials by the action of water: experimental and archaeological reassessment of the
934 orientation patterns at the Olduvai sites . *Journal of Archaeological Science* 41 (0),
935 44 – 68.
- 936 Eren, M. I., Durant, A., Neudorf, C., Haslam, M., Shipton, C., Bora, J., Korisettar,
937 R., Petraglia, M., 2010. Experimental examination of animal trampling effects on
938 artifact movement in dry and water saturated substrates: a test case from South India.
939 *Journal of Archaeological Science* 37 (12), 3010 – 3021.
- 940 García-Moreno, A., Smith, G. M., Kindler, L., Pop, E., Roebroeks, W., Gaudzinski-
941 Windheuser, S., Klinkenberg, V., 2016. Evaluating the incidence of hydrological
942 processes during site formation through orientation analysis. A case study of the
943 middle Palaeolithic Lakeland site of Neumark-Nord 2 (Germany). *Journal of Ar-
944 chaeological Science: Reports* 6, 82 – 93.

- 945 Giusti, D., Arzarello, M., 2016. The need for a taphonomic perspective in spatial analy-
946 sis: Formation processes at the Early Pleistocene site of Pirro Nord (P13), Apricena,
947 Italy. *Journal of Archaeological Science: Reports* 8, 235 – 249.
- 948 Harvati, K., Panagopoulou, E., Tourloukis, V., Thompson, N., Karkanas, P., Athanas-
949 siou, A., Konidaris, G., Tsartsidou, G., Giusti, D., 2016. New Middle Pleistocene
950 elephant butchering site from Greece. In: Paleoanthropology Society Meeting. At-
951 lanta, Georgia, pp. A14–A15.
- 952 Hivernel, F., Hodder, I., 1984. Analysis of artifact distribution at Ngenym (Kenya):
953 depositional and postdepositional effects. In: Hietala, H., Larson, P. (Eds.), *Intrasite*
954 *Spatial Analysis in Archaeology*. Cambridge University Press, Ch. 7, pp. 97–115.
- 955 Hodder, I., Orton, C., 1976. *Spatial Analysis in Archaeology. New Studies in Archaeo-*
956 *logy*. Cambridge University Press, Cambridge.
- 957 Hovers, E., Ekshtain, R., Greenbaum, N., Malinsky-Buller, A., Nir, N., Yeshurun, R.,
958 2014. Islands in a stream? Reconstructing site formation processes in the late Mid-
959 dle Paleolithic site of 'Ein Qashish, northern Israel. *Quaternary International* (0), –.
960 URL [http://www.sciencedirect.com/science/article/pii/
961 S1040618214000433](http://www.sciencedirect.com/science/article/pii/S1040618214000433)
- 962 Isaac, G. L., 1967. Towards the interpretation of occupation debris: Some experiments
963 and observations. *Kroeber Anthropological Society Papers* 37 (37), 31–57.
- 964 Jammalamadaka, S., Sengupta, A., Sengupta, A., 2001. *Topics in Circular Statistics.*
965 Series on multivariate analysis. World Scientific.
- 966 Lenoble, A., Bertran, P., 2004. Fabric of Palaeolithic levels: methods and implications
967 for site formation processes. *Journal of Archaeological Science* 31 (4), 457 – 469.
- 968 Lenoble, A., Bertran, P., Lacrampe, F., 2008. Solifluction-induced modifications
969 of archaeological levels: simulation based on experimental data from a modern
970 periglacial slope and application to French Palaeolithic sites. *Journal of Archaeo-*
971 *logical Science* 35 (1), 99 – 110.
- 972 Malinsky-Buller, A., Hovers, E., Marder, O., 2011. Making time: ‘Living floors’,
973 ‘palimpsests’ and site formation processes – A perspective from the open-air Lower
974 Paleolithic site of Revadim Quarry, Israel. *Journal of Anthropological Archaeology*
975 30 (2), 89 – 101.
976 URL [http://www.sciencedirect.com/science/article/pii/
977 S0278416510000632](http://www.sciencedirect.com/science/article/pii/S0278416510000632)
- 978 Marwick, B., 2017. Computational reproducibility in archaeological research: Ba-
979 sic principles and a case study of their implementation. *Journal of Archaeological*
980 *Method and Theory* 24 (2), 424–450.
- 981 Marwick, B., d'Alpoim Guedes, J., Barton, C. M., Bates, L. A., Baxter, M., Beavan,
982 A., Bollwerk, E. A., Bocinsky, R. K., Brughams, T., Carter, A. K., Conrad, C.,
983 Contreras, D. A., Costa, S., Crema, E. R., Daggett, A., Davies, B., Drake, B. L.,

- 984 Dye, T. S., France, P., Fullager, R., Giusti, D., Graham, S., Harris, M. D., Hawks, J.,
985 Heath, S., Huffer, D., Kansa, E. C., Kansa, S. W., Madsen, M. E., Melcher, J., Negre,
986 J., Neiman, F. D., Opitz, R., Orton, D. C., Przystupa, P., Raviele, M., Riel-Salvatore,
987 J., Riris, P., Romanowska, I., Smith, J., Strupler, N., Ullah, I. I., Vlack, H. G. V.,
988 VanValkenberg, N., Watrall, E. C., Webster, C., Wells, J., Winters, J., Wren, C. D.,
989 2017. Open science in archaeology. *SAA Archaeological Record* 17 (4), 8–14.
990 URL <http://bit.ly/OSIG-SAAAR>
- 991 McPherron, S. J., 2005. Artifact orientations and site formation processes from total
992 station proveniences. *Journal of Archaeological Science* 32 (7), 1003 – 1014.
- 993 Morton, A. G. T., 2004. Archaeological Site Formation: Understanding Lake Margin
994 Contexts. No. 1211 in BAR International Series. Archaeopress, Oxford.
- 995 Nickel, B., Riegel, W., Schonherr, T., Velitzelos, E., 1996. Environments of coal forma-
996 tion in the Pleistocene lignite at Megalopolis, Peloponnese (Greece) - reconstruc-
997 tion from palynological and petrological investigations. *N. Jb. Geol. Palaont. A.* 200,
998 201–220.
- 999 Ohser, J., 1983. On estimators for the reduced second moment measure of point pro-
1000 cesses. *Mathematische Operationsforschung und Statistik, series Statistics* 14, 63–
1001 71.
- 1002 Organista, E., Domínguez-Rodrigo, M., Yravedra, J., Uribe Larrea, D., Arriaza, M. C.,
1003 Ortega, M. C., Mabulla, A., Gidna, A., Baquedano, E., 2017. Biotic and abiotic pro-
1004 cesses affecting the formation of BK Level 4c (Bed II, Olduvai Gorge) and their bear-
1005 ing on hominin behavior at the site. *Palaeogeography, Palaeoclimatology, Palaeo-
1006 ecology*, –.
- 1007 Orton, C., 1982. Stochastic process and archaeological mechanism in spatial analysis.
1008 *Journal of Archaeological Science* 9 (1), 1 – 23.
- 1009 Panagopoulou, E., Tourloukis, V., Thompson, N., Athanassiou, A., Tsartsidou, G.,
1010 Konidaris, G., Giusti, D., Karkanas, P., Harvati, K., 2015. Marathousa 1: a new Mid-
1011 dle Pleistocene archaeological site from Greece. *Antiquity Project Gallery* 89 (343).
- 1012 Petraglia, M. D., Nash, D. T., 1987. The impact of fluvial processes on experimen-
1013 tal sites. In: Nash, D. T., Petraglia, M. D. (Eds.), *Natural formation processes and*
1014 *the archaeological record*. Vol. 352 of International Series. British Archaeological
1015 Reports, Oxford, pp. 108–130.
- 1016 Petraglia, M. D., Potts, R., 1994. Water Flow and the Formation of Early Pleistocene
1017 Artifact Sites in Olduvai Gorge, Tanzania . *Journal of Anthropological Archaeology*
1018 13 (3), 228 – 254.
- 1019 Pierson, T. C., 2005. Distinguishing between debris flows and floods from field evi-
1020 dence in small watersheds. Usgs numbered series, U.S. Geological Survey.
- 1021 R Core Team, 2016. R: A Language and Environment for Statistical Computing. R
1022 Foundation for Statistical Computing, Vienna, Austria.

- 1023 Ripley, B., 1977. Modelling spatial patterns. *Journal of the Royal Statistical Society, series B* 39, 172–212.
- 1025 Ripley, B., 1988. *Statistical inference for spatial processes*. Cambridge University Press.
- 1027 Ripley, B. D., 1976. The second-order analysis of stationary point processes. *Journal of Applied Probability* 13 (2), 255–266.
- 1029 Ripley, B. D., 1981. *Spatial Statistics*. John Wiley and Sons, New York.
- 1030 Schick, K. D., 1984. Processes of paleolithic site formation: an experimental study. Ph.D. thesis, University of California, Berkeley.
- 1032 Schick, K. D., 1986. Stone Age sites in the making: experiments in the formation and transformation of archaeological occurrences. Vol. 319 of International Series. British Archaeological Reports, Oxford.
- 1035 Schick, K. D., 1987. Modeling the formation of Early Stone Age artifact concentrations. *Journal of Human Evolution* 16, 789–807.
- 1037 Schiffer, M. B., 1972. Archaeological Context and Systemic Context. *American Antiquity* 37 (2), 156–165.
- 1039 Schiffer, M. B., 1983. Toward the identification of formation processes. *American Antiquity* 48 (4), 675–706.
- 1041 Schiffer, M. B., 1987. Formation processes of the archaeological record. University of New Mexico Press, Albuquerque.
- 1043 Shackley, M. L., 1978. The behaviour of artefacts as sedimentary particles in a fluvial environment. *Archaeometry* 20 (1), 55–61.
- 1045 Sánchez-Romero, L., Benito-Calvo, A., Pérez-González, A., Santonja, M., 12 2016. Assessment of Accumulation Processes at the Middle Pleistocene Site of Ambrona (Soria, Spain). Density and Orientation Patterns in Spatial Datasets Derived from Excavations Conducted from the 1960s to the Present. *PLOS ONE* 11 (12), 1–27.
- 1049 Texier, J.-P., 2000. A propos des processus de formation des sites préhistoriques / About prehistoric site formation processes. *Paléo* 12 (1), 379–386.
- 1051 URL http://www.persee.fr/web/revues/home/prescript/article/pal_1145-3370_2000_num_12_1_1610
- 1053 van Vugt, N., de Bruijn, H., van Kolfschoten, M., Langereis, C. G., 2000. Magneto- and cyclostratigraphy and mammal-fauna's of the Pleistocene lacustrine Megalopolis Basin, Peloponnesos, Greece. *Geologica Ultrajectina* 189, 69–92.
- 1056 Vaquero, M., Chacón, M. G., García-Antón, M. D., de Soler, B. G., Martínez, K., Cuartero, F., 2012. Time and space in the formation of lithic assemblages: The example of Abric Romaní Level J. *Quaternary International* 247 (0), 162 – 181.

- 1059 Villa, P., 2004. Taphonomy and stratigraphy in european prehistory. Before Farming
1060 2004 (1), 1–20.
1061 URL <https://doi.org/10.3828/bfarm.2004.1.1>
- 1062 Voorhies, M., 1966. Taphonomy and population dynamics of an early Pliocene verte-
1063 brate fauna, Knox County, Nebraska. Ph.D. thesis, University of Wyoming.
- 1064 Walter, M. J., Trauth, M. H., 2013. A {MATLAB} based orientation analysis of
1065 acheulean handaxe accumulations in olorgesailie and kariandusi, kenya rift. Jour-
1066 nal of Human Evolution 64 (6), 569 – 581.
- 1067 Wood, R. W., Johnson, D. L., 1978. A survey of disturbance processes in archaeologi-
1068 cal site formation. In: Schiffer, M. B. (Ed.), Advances in archaeological method and
1069 theory. Vol. 1. Academic Press, Ch. 9, pp. 315–381.
- 1070 Woodcock, N., Naylor, M., 1983. Randomness testing in three-dimensional orientation
1071 data. Journal of Structural Geology 5 (5), 539 – 548.